Determining the electronic states that contribute most to solid-state high-order harmonic radiation

M. Kolesik

James Wyant College of Optical Sciences, University of Arizona, Tucson, Arizona 85721, USA

Utilizing realistic simulations of high-order harmonic generation (HHG) in several materials, we study how different regions of the Brillouin zone contribute to the nonlinear response. It is often assumed that the electronic trajectories that start in the vicinity of the Γ point are predominantly responsible for the HHG spectrum, but it is shown here that such an approximation is generally inaccurate. While examples can be identified where merely 0.4% of the Brillouin zone produces semiquantitatively accurate HHG spectra, in most situations one must include at least 30%–50% of the Brillouin-zone volume to obtain accurate above-the-gap harmonics. For the harmonic peaks below the band-gap energy, the current-density responses from the entire Brillouin zone must always be integrated. We also identify the minimal set of electronic bands necessary for the construction of reduced but still realistic HHG models. The results should be useful for a number of HHG applications, including all-optical reconstructions of the band structure and light-matter couplings or considerations involving semiclassical approaches to solid-state high-order harmonic radiation.

I. INTRODUCTION

Ever since the first observations of the above-the-gap harmonic generation from a solid-state medium [1], there have been numerous efforts [2] to understand the underlying physics and to utilize this extremely nonlinear effect [3,4] for applications providing insight into the quantum world of materials. Solid-state high-order harmonic generation (HHG) has emerged as a tool to map the band structures of materials and to investigate their dynamics with an unprecedented resolution. However, harnessing its full potential as a probe will require detailed understanding of the contributions from different electronic states. In particular, it is necessary to quantify how different parts of the Brillouin zone contribute to the HHG signal and which bands take part in the dynamics.

As is known, a HHG experiment is unable to discriminate between signals from different electronic states and detects only their collective response as a coherent, i.e., an amplitude-by-amplitude, sum. Even theoretically it is impossible to localize sources of harmonic radiation in the sense that one could assign a specific place in the Brillouin zone that is exclusively responsible for a part of the material response. It is because electronic states exposed to an external field accelerate and acquire time-dependent k vectors. As a consequence, depending on the choice of the frame of reference in the reciprocal space, either the density matrix itself or the material properties (i.e., k-dependent operators including the Hamiltonian and current-density observables) move across the coordinate system. In other words, the process is always nonlocal, because each quantum trajectory travels through a significant portion of the Brillouin zone.

Nevertheless, even with these limitations in mind, the question of where in the Brillouin zone the source of the high-order harmonic signal is has been asked many times by researchers seeking physical insights. While we contend that the full zone should be used in any realistic simulation, there is great value

in the intuition and in various interpretations one can gain by examining the roles of different regions in the Brillouin zone. Indeed, such a standpoint underlines not only some HHG interpretations but also a number of applications, including all-optical reconstruction of the electronic band structure [5–7], characterization of light-matter couplings [8–12], and probing the topological properties of materials [13–16]. The notion of a trajectory often plays a role in these methods. Originally inspired by the success of the strong-field approximation in the HHG from atoms, the three-step model [17–19], its variations [6,20,21], and generalizations [22] were adopted to the solid-state context [23]. A common feature among the semiclassical approaches is that an electron follows a path through the k space as it is accelerated by the external field. While the trajectory endpoint and in particular its local band gap determine the radiated photon energy, the initial point is most often identified as the location of the carrier excitation. This motivates the way we choose to assign the optical response to a place in the Brillouin zone: Keeping in mind the issue of nonlocality of the optical response, we label different induced-current contributions by the initial k vector of electronic states (including all bands) that gave rise to that current. This is similar in spirit to the semiclassical treatment, with an important difference that all bands are accounted for on an equal basis in our simulation, so it is perhaps more accurate to speak about a trajectory of the mixed state described by the density matrix.

The understanding of the relative importance between different trajectories is one of the motivations of this work. Our aim is to identify the region of the Brillouin zone which the initial k points must sample, or fill in, in order to obtain an accurate optical response which compares well with the result obtained from the entirety of the Brillouin zone. In the language of semiclassical interpretations of high-order harmonic generation in solids, we want to examine which important

023503-1

electronic trajectories contribute most to the high-order harmonic radiation.

It is a frequent assumption in semiclassical approaches that there is an excitation step at the start of the trajectory when tunneling from the valence band to the conduction band occurs at or close to the Γ point (or at the location of the minimal energy gap). While it has been pointed out [24] that the minimal-gap location does not necessarily dominate the whole HHG process, the approximation that the interband excitation peaks sharply around the point of the minimal gap is rarely tested in concrete situations (see, however, [16] for a notable exception). This work should provide useful insights into this issue.

We concentrate on three-dimensional materials and utilize realistic numerical simulations to compare how the ensembles of electronic-state trajectories starting from different regions of the Brillouin zone contribute to and shape the high-order harmonic responses. Our results will show that there is a qualitative difference between the behaviors of the below-gap and the above-gap harmonics. While for the lower-order harmonic radiation the contributions from the entire Brillouin zone are always necessary to achieve a quantitatively accurate description, only 30%–50% of the Brillouin-zone volume is sufficient to capture a great majority of the higher-order harmonic radiation. However, it turns out that, at least for the three-dimensional materials, the assumption that the electronic states from around the Γ point contribute most of the HHG response is unrealistic in general.

Such a finding may seem to contradict the fact that the tunneling is by far most likely where the energy gap is minimal. To clarify this issue, we investigate what portion of the excited carriers are actually born in the central part of the Brillouin zone. It will be shown that despite the local tunneling rate being much larger around Γ, the rest of the zone still generates the great majority of the excited carriers. Their collective response to the driving field therefore cannot always be neglected.

We also address the question concerning the minimal set of electronic bands that should be included in a reduced model. While some spectral features can be obtained already with a few bands, accurate results require inclusion of bands in sets that are connected via degenerate points or via avoided band crossings [25,26].

II. MATERIAL MODELS

This work utilizes empirical tight-binding models for several materials with zinc-blende and diamond structures. Most of our simulations were performed for GaAs. Besides the fact that it is an important material, this choice is also motivated by the fact that many experimental results are available for this material (see, e.g., [27,28]). Some of the measurements [28] were previously used to verify the accuracy of the model used in this paper. We have demonstrated that the tight-binding description of GaAs, both with and without spin-orbit coupling, provides a nonlinear optical response which agrees quite well with HHG measurements [29]. It was also shown that the model correctly captures the second-order nonlinearity of the material [30]. In other words, the tight-binding description of GaAs, coupled with the recently introduced HHG simulator
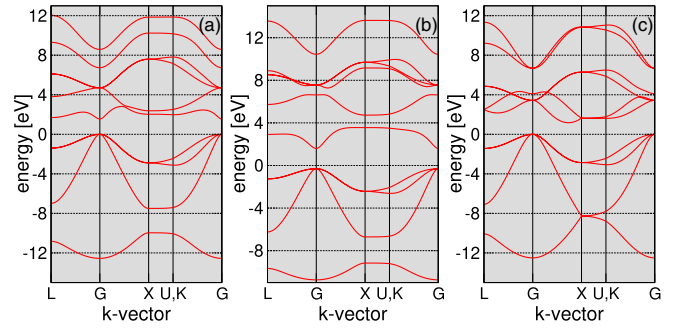

FIG. 1. Electronic band structure of (a) GaAs, (b) CdTe, and (c) Si in the sp^3s^* tight-binding approximation without spin-orbit coupling.

[31], has been tested across the frequency range including below-band-gap and above-band-gap harmonics. This gives us the confidence to draw conclusions from the numerical simulations.

The next material included in our comparative simulations is CdTe. It was recently identified as a medium in which harmonics up to and beyond order of 30 were generated at a very low excitation intensity [32]. The low intensity and flux needed for the high-order harmonic generation makes this material very interesting. It was argued in Ref. [32] that the special feature that makes CdTe distinct is the flatness of its conduction band.

To broaden our set of material models, we choose crystalline silicon as a material which differs from GaAs and CdTe in that it is inversion symmetric. The higher material symmetry eliminates even-order harmonic generation and gives rise to simpler spectra in which it is perhaps easier to investigate which part of the Brillouin zone contributes most. Unlike GaAs, crystalline silicon does not possess a direct gap. Consequently, it is not straightforward to make an argument for a specific location in the Brillouin zone to be the strongest source of high-order harmonic radiation. It should be interesting to see if direct- and indirect-gap media behave differently in this respect.

The description of the materials in this work is based on the same so-called sp^3s^* tight-binding model in [33]. It is applicable to both the zinc-blende and diamond structures. As an input for the structure-gauge-independent SBE (sgiSBE) solver [30,31] which was used to simulate the HHG spectra, the explicit expression for the $\mathbf{k}$-dependent Hamiltonian $h(\mathbf{k})$ was obtained from [34]. The parameter sets were taken from [33] for GaAs and silicon and from [35] for CdTe. For the results shown in what follows, we applied the spin-degenerate version of the material models. Figure 1 illustrates the electronic band structures of the materials investigated in this work.

III. NUMERICAL MODELING OF SOLID-STATE HHG

High-order harmonic generation simulations in this work were done with the sgiSBE. We refer the reader to the descriptions of the algorithm given in [31] and also in [30] and include a brief summary here. For each $\mathbf{k}$ sampling the Brillouin zone, the initial density matrix $\rho_{mn}(\mathbf{k}; t = 0)$ is set

to be the zero-temperature density matrix representing full valence and empty conduction bands. One integration step, or an update from time t_i to time t_{i+1}, can be written as an operator splitting scheme in the form

$$\rho_{mn}(\mathbf{k};t_{i+1}) = \sum_{a,b} \langle m\mathbf{k}_{i+1}|a\mathbf{k}_i\rangle e^{-i\epsilon_a(\mathbf{k}_i)\Delta} \rho_{ab}(\mathbf{k};t_i) e^{+i\epsilon_b(\mathbf{k}_i)\Delta}$$

$$\times \langle b\mathbf{k}_i|n\mathbf{k}_{i+1}\rangle, \qquad (1)$$

where $\Delta = t_{i+1} - t_i$ is the time step; $\mathbf{k}_i = \mathbf{k} - \mathbf{A}(t_i)$, with $\mathbf{A}$ representing the vector potential of the driving pulse; and $|a\mathbf{k}_i\rangle$ stands for the $\mathbf{k}$-dependent Bloch eigenstate in the electronic band a. The middle terms in (1) can be understood as the first split step which evolves the density matrix in the current Hamiltonian eigenbasis $\{|a\mathbf{k_i}\rangle\}$. For the next split step, the new-time eigenbasis $\{|b\mathbf{k}_{i+1}\rangle\}$ is obtained by the exact diagonalization of the Hamiltonian $h(\mathbf{k}_{i+1})$, and then the density matrix is transformed into the new basis as shown in the first and last terms in (1). This update scheme is applied in parallel, independently for all $\mathbf{k}$ sampling the Brillouin zone. Dephasing is approximated as usual, in a separate split step

$$\rho_{mn}(\mathbf{k};t) \leftarrow \rho_{mn}(\mathbf{k};t) \exp(-\Delta t/T_2), \qquad (2)$$

with T_2 the dephasing time, which we set equal to 5 fs; note that the observations we arrive at in this work are independent of its precise value.

The total observed current density is calculated as an integral over the complete Brillouin zone

$$\mathbf{j}(t) = \sum_{mn} \int_{BZ} \frac{d\mathbf{k}}{(2\pi)^3} \langle n\mathbf{k}_t|\partial_{\mathbf{k}_t} h(\mathbf{k}_t)|m\mathbf{k}_t\rangle \rho_{mn}(\mathbf{k};t), \qquad (3)$$

where the Hamiltonian gradient $\partial_{\mathbf{k}_t} h(\mathbf{k}_t)$ is obtained from the tight-binding model in an analytic form, and its matrix element in the above formula represents the operator observable corresponding to the total current density. It should be emphasized that this formulation for the observed current density is general and does not depend on any specifics of the model. While we choose to adopt the notation from [36], this expression is equivalent to those utilizing derivatives of the operator's matrix elements such as in, e.g., [37]. For simplicity, we do not decompose $\mathbf{j}(t)$ into intra- and interband currents.

An important aspect of the method is the grid of $\mathbf{k}$ vectors sampling the Brillouin zone, which must be sufficiently dense for the integral (3) to converge. The convergence properties with respect to the Brillouin-zone sampling density were discussed in detail in [29]. For this work, we sample the reciprocal-space cell with an equidistant grid of 128^3 grid points. The grid is aligned with the reciprocal basis vectors and it is invariant under the symmetry operations of the material.

IV. SIMULATION RESULTS

A. Response from a portion of the Brillouin zone

For a crystalline sample with a fixed orientation, we assume a linearly polarized optical pulse driving the current-density response, which is subsequently converted into a spectrum. For a given $\mathbf{k}$, the integrand in (3) represents the contribution of this $\mathbf{k}$ spot inside the Brillouin zone to the total response. Because it is often assumed that $\mathbf{k}$ in the close vicinity of Γ contribute most to the HHG spectrum, we define a partially sampled current density as

$$\mathbf{j}(r,t) = \sum_{mn} \int_{BZ,|\mathbf{k}|<r} \frac{d\mathbf{k}}{(2\pi)^3} \langle n\mathbf{k}_t|\partial_{\mathbf{k}_t} h(\mathbf{k}_t)|m\mathbf{k}_t\rangle \rho_{mn}(\mathbf{k};t).$$

$$(4)$$

In other words, for a given radius r we only include the current-density contributions from the initial $\mathbf{k}$ vectors that are closer to Γ than r. The central question in what follows is how large r must be for $\mathbf{j}(r,t)$ to be an accurate approximation of the total current density $\mathbf{j}(t)$.

B. HHG from the vicinity of the Γ point

Motivated by the assumption that high-order harmonic radiation is mostly mediated by the electronic states which are initially close to the Γ point of the Brillouin zone, we first look at the spectra generated by such states. We select a portion of the zone with a radius of $r = 1$ (in units of inverse lattice constant) and calculate their collective contribution to $\mathbf{j}(r = 1, t)$ and then the corresponding HHG spectrum. During this and the following simulations, we make sure that all symmetry-related $\mathbf{k}$ points are simultaneously included so that the calculated response has the correct material symmetry. This particular (i.e., for $r = 1$) symmetry-respecting Γ vicinity contains only about 0.4% of the total Brillouin-zone volume, so it is rather small.

As a first example, take GaAs excited by a 3.5-µm pulse with the electric-field amplitude of 8.7 MV/cm, polarized in the [011] direction. For this sample orientation, one expects the odd harmonics to be p polarized, i.e., parallel to the excitation, while the even harmonics should be s polarized.

Figure 2 shows the simulated HHG spectra, generated by the electronic states that are initially in the Γ vicinity, compared to the spectrum in which the entirety of the Brillouin zone was included. For the p polarization, the two HHG spectra are quite similar. Keeping in mind that the scale of the figure is logarithmic, one can see that the largest deviations between the two spectra are about one order of magnitude or only slightly larger. For the s-polarized response, the gap between the partial and total spectra opens a bit more, especially for the second harmonic and the harmonics above the order of 18. Nevertheless, the fact that contributions from trajectories with initial points covering mere 0.4% of the Brillouin-zone volume produce a HHG response so close to the total suggests that the Γ point indeed dominates the HHG process, as is often assumed in various semiclassical analyses.

This is an encouraging observation, but it would be premature to conclude that the prominence of the Γ point as the HHG source is a typical behavior. For the next example, the excitation wavelength is chosen twice as long, $\lambda = 7$ µm. The expectation is perhaps that in response to longer wavelengths a small vicinity of the Brillouin-zone center also generates most of the harmonic power. Indeed, one could argue that a longer wavelength implies a more off-resonant tunneling excitation of electrons into the conduction bands, which should translate into carriers being born in a tighter neighborhood of Γ. As a result, an even smaller portion of the Brillouin zone could be responsible for the harmonic response.
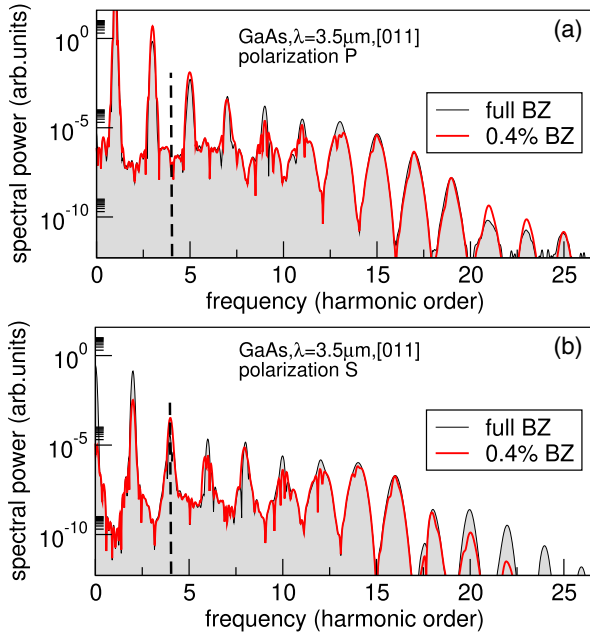
FIG. 2. GaAs high-order harmonic spectrum from the full Brillouin zone (black, gray-filled line) compared to that generated in the vicinity of the Γ point encompassing 0.4% of the total Brillouin-zone volume (red line) for (a) parallel and (b) perpendicular polarization. The excitation pulse, at $\lambda = 3.5$ μm wavelength, is polarized in the $y = z$ direction. The vertical dashed line in this and the following figures marks the frequency corresponding to the band-gap energy of the material.
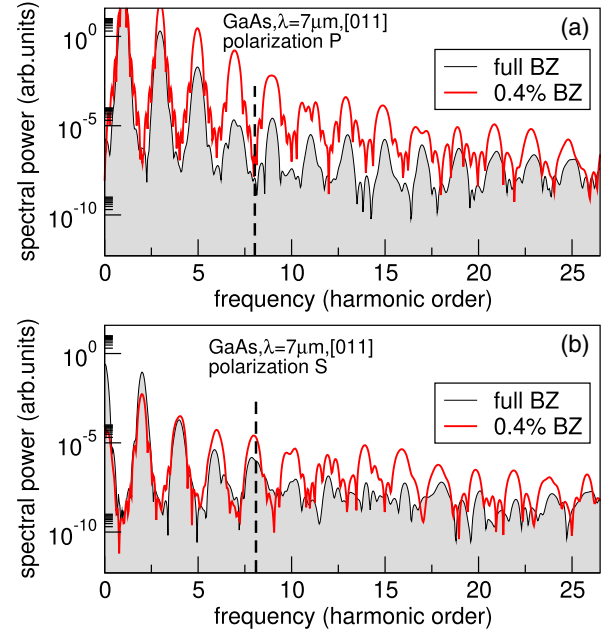

FIG. 3. GaAs high-order harmonic spectrum from the full Brillouin zone (black, gray-filled line) compared to that generated in the vicinity of the Γ point encompassing 0.4% of the total Brillouin-zone volume (red line) for (a) parallel and (b) perpendicular polarization. The excitation pulse, at $\lambda = 7$ μm wavelength, is polarized in the $y = z$ direction.

However, Fig. 3 shows otherwise. While all conditions with the exception of the excitation wavelength are exactly the same as in the former example, one can see a dramatic difference between the partial and full spectra. The gap between the two opens even more dramatically for yet longer driving wavelength $\lambda = 10$ μm, as the example in Fig. 4 shows. So the argument given in the preceding paragraph which invokes the less resonant excitation does not really work. Looking for a reason why, one may consider the effect the wavelength has on the carrier travel through the k space. The amplitude of the oscillation is indeed twice as large in the simulation with $\lambda = 7$ μm than in that with $\lambda = 3.5$ μm. It is therefore tempting to run the same simulation with a driving amplitude decreased such that the k-space oscillations are exactly the same as for the shorter wavelength illustrated in Fig. 2. The results are reported in Fig. 5, showing that while one can see a much better resemblance between the partial and full HHG spectra in this case, there still remains a sizable gap of several orders between certain harmonic peaks. Moreover, the weaker excitation produces a much less developed harmonic spectrum, so going to even lower driving amplitudes makes little sense. The takeaway here is therefore that a weaker pump alone does not ensure that the trajectories originating in the central part of the Brillouin zone dominate the HHG spectrum.

It turns out that the behavior shown in Fig. 3 is more typical than that shown in Fig. 2. Figure 6 shows an analogous comparison of partial- and full-zone spectra for CdTe. A recent study showed that the high-order harmonic generation

is significantly stronger in this material and the relatively flat conduction-band shape was identified as a possible reason. The higher density of states around Γ should further emphasize its contribution to the response, and this is why the material was selected for our next example. Here we have chosen to change the excitation-pulse polarization to [111], for which both even and odd harmonics appear in the p polarization, while the s-polarized response vanishes. The figure shows a range of frequencies similar to that observed in the experiments [32]. In qualitative agreement with the experiment, a rather strong set of harmonics forms between order 20 and 30 and their relative powers appear to be within reasonable limits. We therefore trust that this simulation also
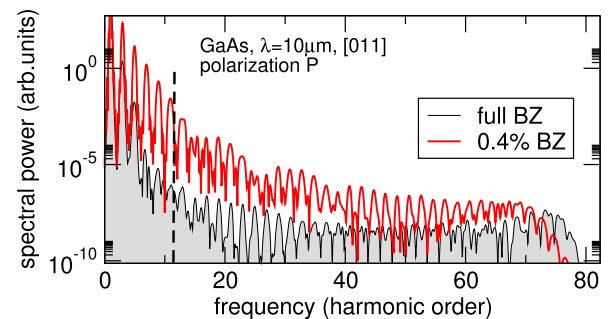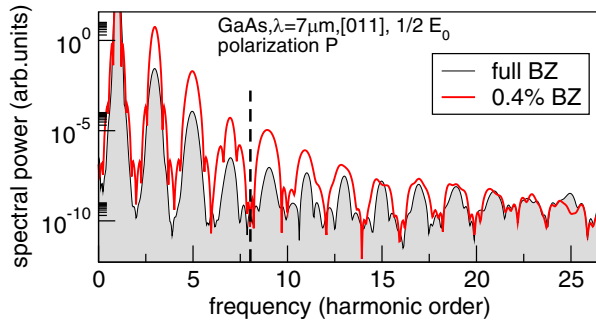

FIG. 4. GaAs high-order harmonic spectrum from the full Brillouin zone (black, gray-filled line) compared to that generated in the vicinity of the Γ point encompassing 0.4% of the total Brillouin-zone volume (red line). The excitation pulse, at $\lambda = 10$ μm wavelength, is polarized in the $y = z$ direction.

FIG. 5. GaAs high-order harmonic spectrum from the full Brillouin zone (black, gray-filled line) compared to that generated in the vicinity of the Γ point encompassing 0.4% of the total Brillouin-zone volume (red line). The conditions are as in Fig. 3, except the field amplitude is reduced to $\frac{1}{2}$.

FIG. 7. Silicon high-order harmonic spectrum from the full Brillouin zone (black, gray-filled line) compared to that generated in the vicinity of the Γ point encompassing 0.4% of the total Brillouin-zone volume (red line). The excitation pulse, at $\lambda = 7$ μm wavelength, is polarized in the $x = y = z$ direction.

is sufficiently realistic. The important takeaway from this numerical experiment is that the small central portion of the Brillouin zone provides a poor approximation of the actual HHG spectrum. While the qualitative shape and relative peak powers are qualitatively very similar between the two spectra, the partial response is orders of magnitude stronger.

As yet another example, we choose crystalline silicon as an inversion-symmetric material with an indirect band gap. The sample orientation and the properties of the excitation pulse are the same as in the previous case, i.e., $\lambda = 7$ μm, and the electric-field oscillation direction is [1,1,1]. Figure 7 shows once again that the immediate neighborhood of Γ does not produce a HHG response which could be compared to that from the full Brillouin zone. One could even argue that the difference here is larger than that in the previous examples. Indeed, the harmonic orders 7–11 appear to be four to five orders of magnitude stronger than those generated from the full Brillouin zone. We speculate that this could be the manifestation of the indirect gap of this material.

To summarize this section, we have shown that the high-order harmonic spectra generated from electronic states that initially reside in a small neighborhood of the Brillouin-zone center are not, at least not in general, a good approximation of the full response. Thus, one needs to go beyond the immediate
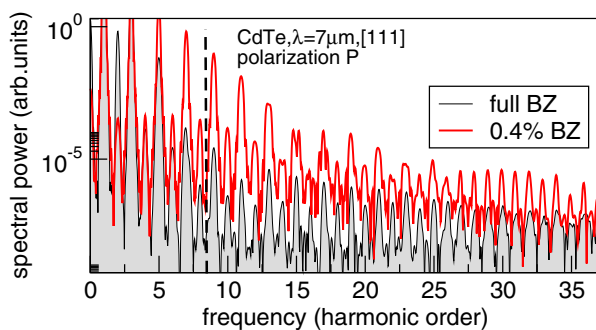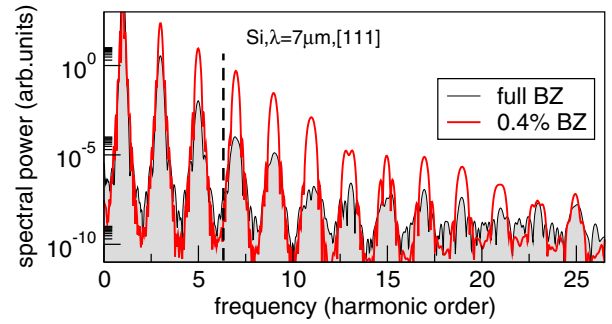
vicinity of the Γ point to obtain a more precise representation of the HHG spectra. In the following section we quantify how large the integration region should be.

C. Mapping the HHG sources

In order to map the strength of the HHG source across the Brillouin zone, we set up a series of simulations for each of the studied materials. We increase the radius r of the Γ-centered subset of the Brillouin zone in steps of $1a^{-1}$, calculating the current density $\mathbf{j}(r, t)$ and the corresponding spectrum $S(r, \omega)$ at each step, until the entirety of the zone is included. Note that the values $r = \{1, 2, 3, 4, 5, 6, 7\}a^{-1}$ represent 0.4%, 3.4%, 11%, 27%, 54%, 86%, and 99.99%, respectively, of the full-zone volume. The goal of this mapping is to identify how large a portion of the Brillouin zone must be included and populated by the initial states for a reasonably accurate HHG simulation.

For the sake of visualization, the integrated harmonic-band power $P(r, h)$ is calculated from the simulated spectrum $S(r, \omega)$ in the given simulation as $P(r, h) = \int_{(h-0.5)\omega_0}^{(h+0.5)\omega_0} |S(r, \omega)|^2 d\omega$. The integration interval is always centered on the integer multiple of the fundamental frequency ω_0, whether that particular harmonics is allowed by symmetry or not, and the interval is one harmonic order wide. The two-dimensional maps of $R(r, h) = P(r, h)/P(r = 8, h)$ are plotted versus the order h and $r \in (1, 8)a^{-1}$. This quantity, or more precisely its approach to unity, reflects the spectrum convergence since for $r = 8$ the entire Brillouin zone is already included in the integration. (Note that $r \approx 7.025$, corresponding to $|\Gamma W|$, represents the entire zone.) To make the resulting graphs easier to interpret, at least for their global features, the interpolation order of the plot routine is set equal to three (resulting in an artificially smooth plotted surface). Since the logarithmic scale is natural for simulated spectra, $\log_{10}[R(r, h)]$ is depicted in the following two figures.

Figure 8 illustrates the convergence of the simulated spectrum with the increasing radius r of the portion of the Brillouin zone included in the simulation. The material here is GaAs and all conditions are the same as for Fig. 2. Thus, this figure shows how the red curves in Fig. 2 gradually approach (with increasing r) the black curves corresponding to the full-zone spectrum.
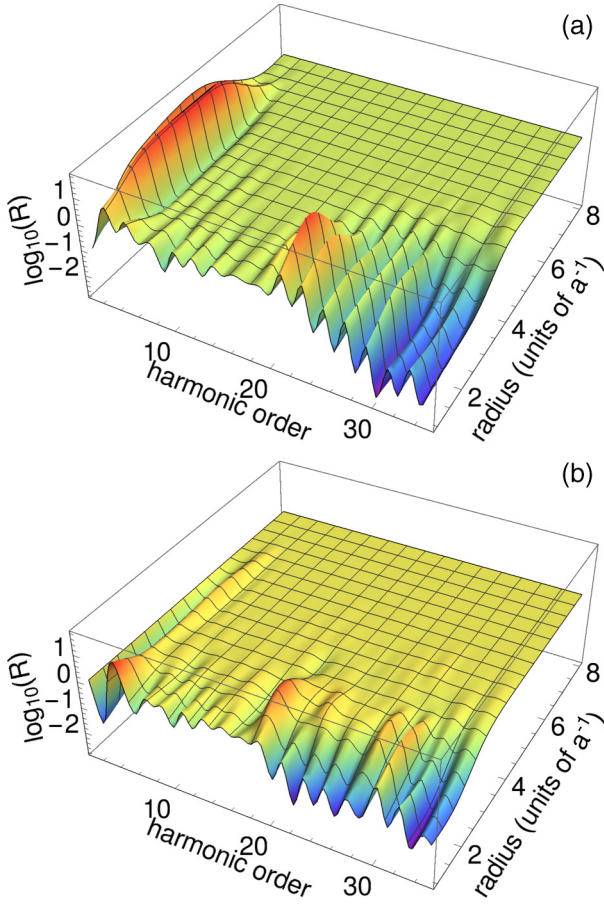

FIG. 6. CdTe high-order harmonic spectrum from the full Brillouin zone (black, gray-filled line) compared to that generated in the vicinity of the Γ point encompassing 0.4% of the total Brillouin-zone volume (red line). The excitation pulse, at $\lambda = 7$ μm wavelength, is polarized in the $x = y = z$ direction.

FIG. 8. Convergence of the simulated spectrum for GaAs excited in the [011] direction at $\lambda = 3.5$ μm (as in Fig. 2). The quantity $\log_{10}[R(r, h)]$ (see the text for details), representing the ratio of the partial- ($r < 7.025\ldots$) to full-zone spectral power integrated over the harmonic band h, is shown on a logarithmic scale. Results are shown for the (a) p- and (b) s-polarized HHG spectra.

FIG. 9. Simulated spectrum convergence for GaAs excited in the [011] direction at $\lambda = 7$ μm (as in Fig. 3) for (a) the p-polarized response and (b) the s-polarized response.

Several features become evident. First, the below-gap harmonics are never accurate until $r \approx 7a^{-1}$, i.e., essentially until the entire zone is included in the simulation. Second, for the higher-order harmonics it takes $r \approx 4a^{-1}$, i.e., about 25% of the full-zone volume, to obtain an accurately simulated spectrum. Third, while quantitatively different, the convergence behaviors of the p- and s-polarized responses are similar.

Figure 9 shows similar results for the longer excitation wavelength $\lambda = 7$ μm and corresponds to the transition between the extreme cases depicted in Fig. 3. Comparison to Fig. 8 shows that while the small-r results are an order of magnitude less accurate (note the different vertical scale in the two figures), a good convergence (but for higher-order harmonic only) is achieved at about the same rate, and perhaps even faster at the high-frequency end of the spectrum. We note that the convergence behavior is very similar also in the cases of silicon and CdTe, and this is illustrated Fig. 10, where Figs. 10(a) and 10(b) correspond to Figs. 6 and 7, respectively.

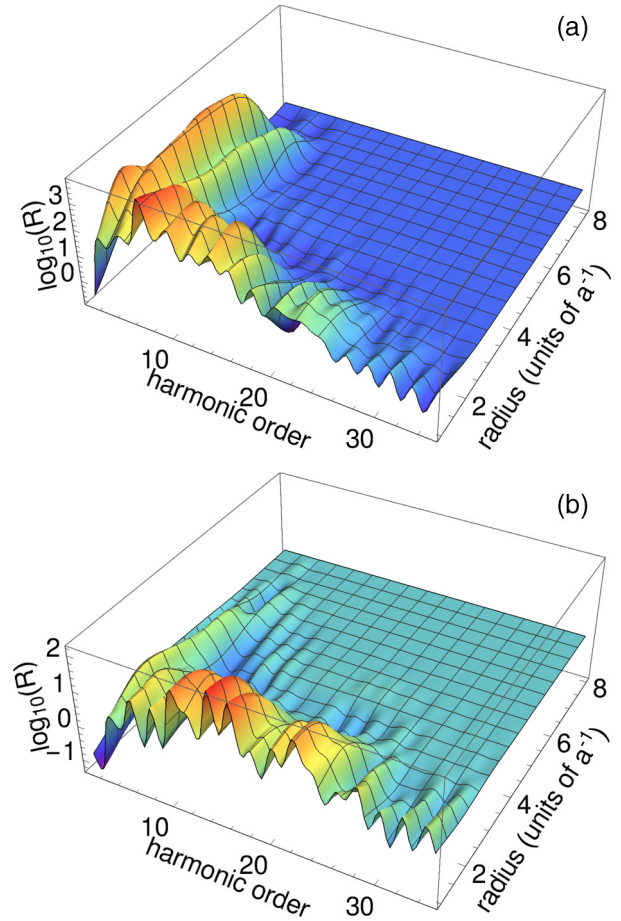For a more quantitative representation of the convergence of the simulated spectra as functions of the portion of the Brillouin zone included, Figs. 11 and 12 show the ratio $R(r, h) = P(r, h)/P(r = 8, h)$ between the partial-spectrum and full-spectrum power integrated over the given harmonic band. Figures 11(c) and 12(c) show that the lower-order harmonics cannot be obtained accurately unless the entire zone is integrated. The medium-high harmonic orders [shown in Figs. 11(b) and 12(b)] converge faster, with the partial-zone results accurate within an order of magnitude once the integrated zone portion is larger than about one-third. The high-order harmonics [Figs. 11(a) and 12(a)] become quite accurate already at about 25%–50% of the entire zone included.

So, to answer the question about the size of the zone that needs to be included in the simulation, it is 100% and roughly 50% for the below-gap and the above-gap harmonics, respectively. From the simulation standpoint, a 50% increase in speed is probably not worth the trouble.

On the other hand, this result is important for the interpretations of HHG dynamics in those cases where any kind of trajectory comes into consideration. It indicates that the starting points of the contributing trajectories should cover at least 30%–50% of the Brillouin-zone volume and that the corresponding contributions should be coherently added up to represent the total response of the material.
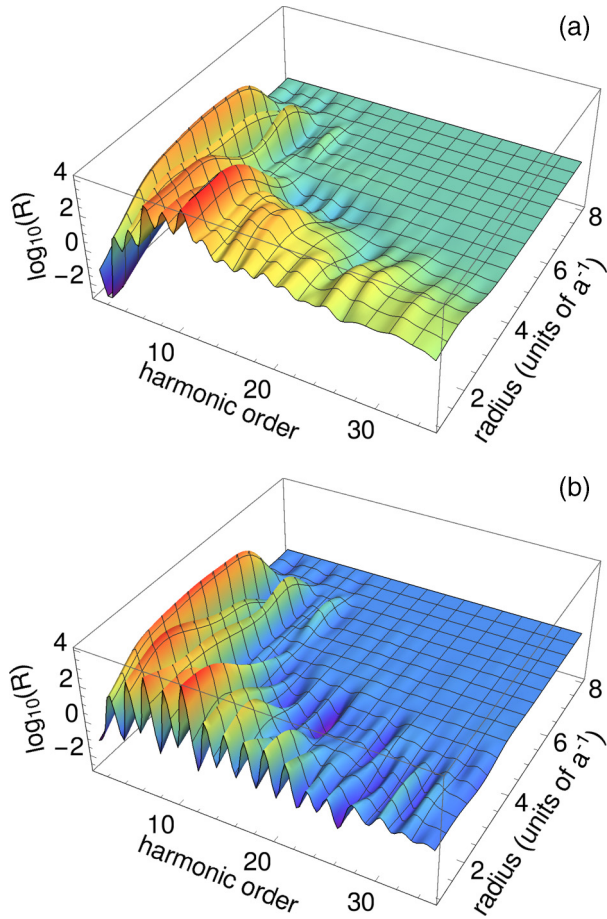
FIG. 10. Convergence of the simulated spectrum of the *p*-polarized response for (a) CdTe (as in Fig. 6) and (b) Si (as in Fig. 7).

D. Mapping the tunneling rate

The finding that the Brillouin zone center in general does not contribute most of the HHG response seems to contradict the highest tunneling probability in this region. Indeed, if the valence- to conduction-band excitation does behave as the tunneling ionization in atoms, then the rate of excitation should be exponentially sensitive to the k-dependent band gap and therefore fall off quickly upon departure from the zone center. Based on this argument, one sometimes assumes that the carriers are only created at the point of the minimal gap.

The explanation is actually very simple. It turns out that the difference between the tunneling rates is counteracted by the fact that the volume of the Brillouin zone overshadows the vicinity of the Γ point. To illustrate this, we have measured the total population in all conduction bands combined. Figure 13 shows the result for the examples of GaAs and CdTe excited with a $\lambda = 7$ µm pulse. Figure 13(a) makes a case for the great majority of carriers being generated away from the Γ point. Figure 13(b) depicts the total excited population in the integrated subset of the Brillouin zone divided by the volume of the latter. As such it is a measure of the (averaged) tunneling rate. This quantity indeed shows that the excitation rate is greatly larger around the zone center, precisely as expected.
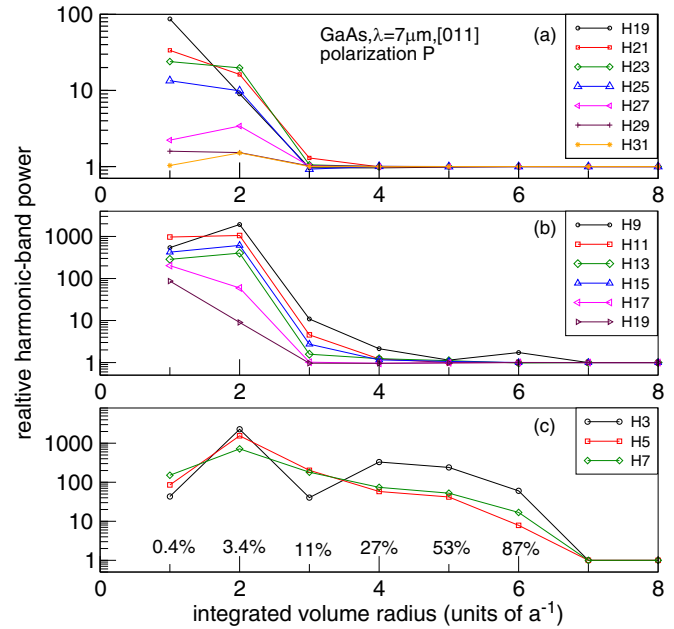

FIG. 11. Convergence of the *p*-polarized HHG spectrum for GaAs excited by a pulse polarized in the $y = z$ direction at $\lambda = 7$ µm. Shown is the ratio $R(r, h)$ between the spectral power (integrated over a harmonic band) obtained from a portion of the Brillouin zone and the corresponding power for the entire zone. Lines connecting the symbols serve as a guide for the eye. Percentages shown in (c) represent the volume portion of the whole zone.

It is just that the contrast is not large enough to compensate for the much bigger volume of the peripheral regions of the Brillouin zone.
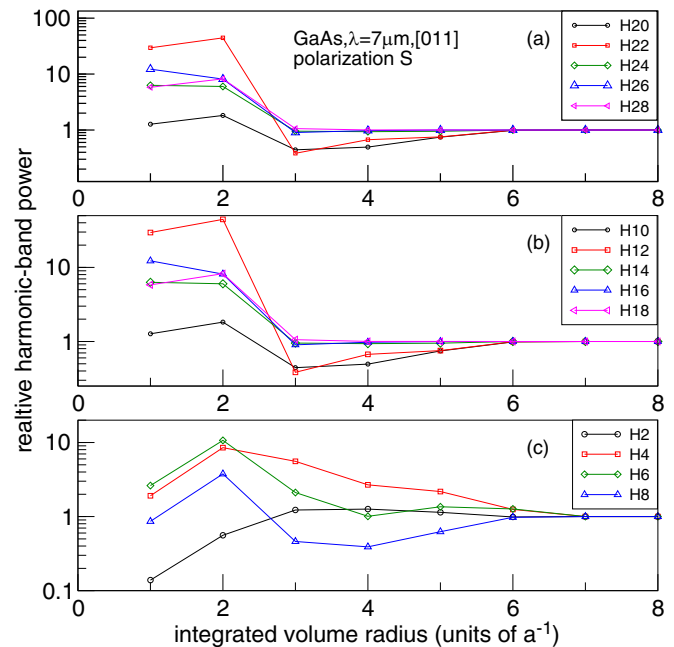

FIG. 12. Convergence of the *s*-polarized HHG spectrum for the same conditions as in Fig. 11.
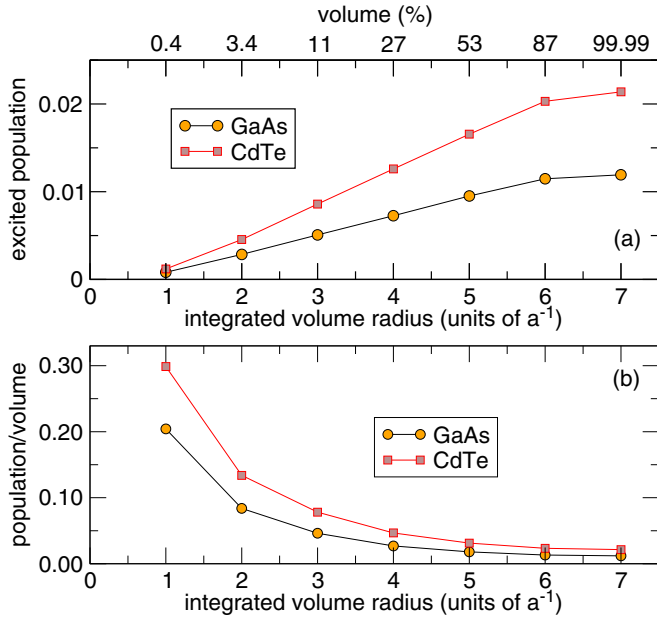
FIG. 13. (a) Total population fraction of excited states inside the reciprocal-space integration volume centered on the Γ point. The top horizontal axis shows the size of the volume as a percent fraction of the full Brillouin zone. (b) Population divided by the volume which gives the average tunneling rate for the states inside the volume of radius r. As expected, the tunneling rate peaks in the center of the zone.

E. Relevant energy bands

One sometimes makes an argument that a HHG spectrum, or perhaps just one of its peaks, is generated by the contributions from a limited number of electronic bands, possibly from only a single valence-conduction pair. Indeed, this kind of assumption underlies a number of approaches for all-optical reconstruction applied to the band structures or to the k-dependent dipole moments.

To test which electronic bands give relevant contributions in the materials studied here, we have repeated the simulation with restricted sets of states. The restriction is realized by projecting the density matrix [or equivalently by projecting the k-dependent Hamiltonian $h(\mathbf{k})$] onto a subspace spanned by the select bands at each integration step. The results will be illustrated for the case of GaAs, excited with a $\lambda = 3.5$ μm pulse (the situation corresponding to that illustrated in Fig. 2), but the observations are similar in all situations investigated in this work.

First, we select the bands 1–4 (labeling the lowest-energy band as 0). This selection accounts for the three highest valence bands and the lowest-energy conduction band. It seems reasonable to expect that these are the most important bands above and below the gap. We compare the resulting HHG spectrum to that obtained from the full simulation in Fig. 14 for the p-polarized component of the response. It is encouraging that the spectra are quite close to each other for harmonics lower than 19. However, one can see pronounced artifacts at the high-frequency end of the spectrum, where strong harmonic peaks appear which do not exist or which are about five orders of magnitude weaker in the full spectrum.
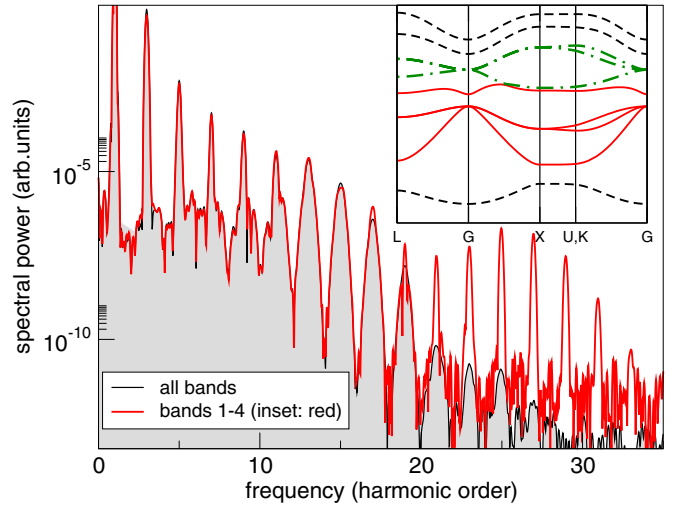

FIG. 14. High-order harmonic spectrum from a reduced model. The black line and gray-shaded area shows the spectrum obtained from the full simulation. The thin red line represents the result of a simulation restricted to the bands shown by red solid lines in the inset.

So if we ask which bands need to be included such that the corresponding spectrum is accurate across all frequencies, the set of 1–4 appears to be inadequate. We speculate that the reason is that the conduction band 4 makes a close approach to the group of higher-energy bands shown by dash-dotted line in the inset of Fig. 14. In a time-dependent external field they become coupled and the populations and polarizations resulting from this coupling affect the dynamics.

Inclusion of the next conduction band does not improve the situation (data not shown); the artifacts at the higher-frequency side of the spectrum actually become slightly worse. Only after including the whole group 5–7 (dark green dash-dotted lines in Fig. 14) do we obtain a HHG spectrum that is very close to the full spectrum with the exception of small deviations for the lowest-order harmonics.

So we arrive at the conclusion that while an individual harmonic peak could be approximated with a limited set of electronic bands, to guarantee the accuracy for all harmonics, one should include all energetically connected bands below and above the band gap. This observation is in line with the band-to-band excitation mechanism described in [25,26].

V. CONCLUSION

Numerical simulations of the high-order harmonic generation in zinc-blende materials GaAs and CdTe and in crystalline silicon were executed for two different excitation wavelengths while gradually including the nonlinear-response contributions from larger and larger portions of the Brillouin zone. The goal of this work was to determine how large the region in the Brillouin zone must be in a numerical simulation in order to produce quantitatively accurate spectra. It turns out that there is no simple answer to the question posed in the title of this work. Nevertheless, our comparative simulations offer

useful insights into certain trends and behaviors which seem quite universal.

The assumption that the Brillouin-zone center dominates the high-order harmonic processes has been used in a number of HHG interpretations, especially those incorporating aspects of semiclassical approaches. However, we have found that this assumption is not justified, at least not in general. While we have identified an example where the Γ neighborhood encompassing merely 0.4% of the Brillouin zone volume does provide a HHG spectrum accurate within one order of magnitude globally and with much better accuracy locally (specifically for the medium-order harmonic orders), we have also found several cases where the contribution from the zone center is orders of magnitude different from the total spectrum. Interestingly, in such cases the central contribution appears to be stronger than that of the whole zone, which indicates that destructive interferences occur across the Brillouin zone.

On the other hand, it turns out that for (only) the above-the-gap frequencies, the center of the zone produced qualitatively correct spectra in all cases studied in this work. The zone-center HHG spectra exhibited stronger peak-to-valley contrast, but the overall spectrum shapes were good. We therefore think that, in light of these results, the approximations restricted to the Γ point (or to a small vicinity of it) remain justified for qualitative investigations into underlying physics. However, it should be emphasized that no matter how small a portion of the Brillouin zone is used, the sampling grid must have the symmetry of the material.

For the simulations which aim for higher accuracy, we conclude that a significant portion of the Brillouin zone must be integrated over. Of course, precisely how large it should be depends on the expected accuracy, material, and excitation wavelength. As a rough estimate, 30%–50% of the zone volume should be included for a simulated spectrum with the harmonic peaks accurate within an order of magnitude or better. In terms of the excitation wavelength, we observed that while the spectra generated from the zone center were more accurate for the shorter wavelength, the convergence toward the full-zone solution seems somewhat faster for the longer wavelength, i.e., a smaller part of the Brillouin zone can suffice.

We trust that these observations will prove useful for a number of applications concerning solid-state high-order harmonic generation, including all-optical band-structure reconstruction and/or optical measurements of Berry curvatures and shift vectors. Analyses which rely on the assumption of specific starting points for the relevant trajectories could be generalized to account for the fact that in reality a distribution or a bundle of trajectories should provide a physically more realistic picture.

Another finding with potential impact on such applications is that care should be exercised when one wants to restrict the number of electronic bands believed to account for the relevant response contributions. We have found that in order to obtain good accuracy across all frequencies, all bands that are connected or that closely approach each other somewhere in the Brillouin zone must be included. In other words, it should be safer to apply various reconstruction algorithms to the whole connected group of electronic bands.

A rather surprising outcome of this study is that the lower-order, below-the-gap harmonics always require the integration of all response contributions across the entirety of the Brillouin zone. This finding is important for the future microscopic-level modeling of laser materials, such as zinc-blende wide-gap semiconductors. Whenever the nonlinear propagation of optical pulses plays a role, the second- and third-order harmonic responses in particular must be sufficiently accurate. This work shows that the Brillouin zone center alone is insufficient to yield an accurate description of the nonlinear properties at frequencies below the gap.

Our work concentrated on the three-dimensional materials and it is not a given that the results apply to the (effectively) two-dimensional systems, where the central part of the Brillouin zone constitutes a much larger fraction of its volume. On one hand, one could argue that such an investigation is less important from the practical standpoint, because even complete sampling of two-dimensional Brillouin zones does not present any significant numerical challenge. On the other hand, it would be interesting to extend the present study to two-dimensional materials for conceptual reasons, for example, to improve the semiclassical interpretations.

ACKNOWLEDGMENT

---

[1] S. Ghimire, A. D. DiChiara, E. Sistrunk, P. Agostini, L. F. DiMauro, and D. A. Reis, Observation of high-order harmonic generation in a bulk crystal, Nat. Phys. **7**, 138 (2011).

[2] J. Park, A. Subramani, S. Kim, and M. F. Ciappina, Recent trends in high-order harmonic generation in solids, Adv. Phys.: X **7**, 2003244 (2022).

[3] S. Ghimire and D. A. Reis, High-harmonic generation from solids, Nat. Phys. **15**, 10 (2019).

[4] E. Goulielmakis and T. Brabec, High harmonic generation in condensed matter, Nat. Photon. **16**, 411 (2022).

[5] G. Vampa, T. J. Hammond, N. Thiré, B. E. Schmidt, F. Légaré, C. R. McDonald, T. Brabec, D. D. Klug, and P. B. Corkum, All-optical reconstruction of crystal band structure, Phys. Rev. Lett. **115**, 193603 (2015).

[6] A. A. Lanin, E. A. Stepanov, A. B. Fedotov, and A. M. Zheltikov, Mapping the electron band structure by intraband high-harmonic generation in solids, Optica **4**, 516 (2017).

[7] A. J. Uzan-Narovlansky, A. Jiménez-Galán, G. Orenstein, R. E. F. Silva, T. Arusi-Parpar, S. Shames, B. D. Bruner, B. Yan, O. Smirnova, M. Ivanov, and N. Dudovich, Observation of light-driven band structure via multiband high-harmonic spectroscopy, Nat. Photon. **16**, 428 (2022).

[8] Y. Qiao, Y.-Q. Huo, S.-C. Jiang, Y.-J. Yang, and J.-G. Chen, All-optical reconstruction of three-band transition dipole moments

by the crystal harmonic spectrum from a two-color laser pulse, Opt. Express **30**, 9971 (2022).

[9] D. Wu, L. Li, Y. Zhan, T. Huang, H. Cui, J. Li, P. Lan, and P. Lu, Determination of transition dipole moments of solids with high-order harmonics driven by multicycle ultrashort pulses, Phys. Rev. A **105**, 063101 (2022).

[10] S. Jiang, H. Wei, J. Chen, C. Yu, R. Lu, and C. D. Lin, Effect of transition dipole phase on high-order-harmonic generation in solid materials, Phys. Rev. A **96**, 053850 (2017).

[11] S. Jiang, J. Chen, H. Wei, C. Yu, R. Lu, and C. D. Lin, Role of the transition dipole amplitude and phase on the generation of odd and even high-order harmonics in crystals, Phys. Rev. Lett. **120**, 253201 (2018).

[12] Y. Qiao, Y. Huo, H. Liang, J. Chen, W. Liu, Y. Yang, and S. Jiang, Robust retrieval method of crystal transition dipole moments by high-order harmonic spectrum, Phys. Rev. B **107**, 075201 (2023).

[13] D. Baykusheva, A. Chacón, J. Lu, T. P. Bailey, J. A. Sobota, H. Soifer, P. S. Kirchmann, C. Rotundu, C. Uher, T. F. Heinz, D. A. Reis, and S. Ghimire, All-optical probe of three-dimensional topological insulators based on high-harmonic generation by circularly polarized laser fields, Nano Lett. **21**, 8970 (2021).

[14] A. J. Uzan, G. Orenstein, A. Jiménez-Galán, C. McDonald, R. E. F. Silva, B. D. Bruner, N. D. Klimkin, V. Blanchet, T. Arusi-Parpar, M. Krüger, A. N. Rubtsov, O. Smirnova, M. Ivanov, B. Yan, T. Brabec, and N. Dudovich, Attosecond spectral singularities in solid-state high-harmonic generation, Nat. Photon. **14**, 183 (2020).

[15] G. Bae, Y. Kim, and J. D. Lee, Revealing Berry curvature of the unoccupied band in high harmonic generation, Phys. Rev. B **106**, 205422 (2022).

[16] C. P. Schmid, L. Weigl, P. Grössing, V. Junk, C. Gorini, S. Schlauderer, S. Ito, M. Meierhofer, N. Hofmann, D. Afanasiev, J. Crewse, K. A. Kokh, O. E. Tereshchenko, J. Güdde, F. Evers, J. Wilhelm, K. Richter, U. Höfer, and R. Huber, Tunable non-integer high-harmonic generation in a topological insulator, Nature (London) **593**, 385 (2021).

[17] G. Vampa, C. R. McDonald, G. Orlando, P. B. Corkum, and T. Brabec, Semiclassical analysis of high harmonic generation in bulk crystals, Phys. Rev. B **91**, 064302 (2015).

[18] G. Vampa and T. Brabec, Merge of high harmonic generation from gases and solids and its implications for attosecond science, J. Phys. B: At. Mol. Opt. Phys. **50**, 083001 (2017).

[19] L. Yue and M. B. Gaarde, Introduction to theory of high-harmonic generation in solids: Tutorial, J. Opt. Soc. Am. B **39**, 535 (2022).

[20] D. Tang and X.-B. Bian, Multiple collisions in crystal high-order harmonic generation, Chin. Phys. B **31**, 123202 (2022).

[21] L. Li, P. Lan, X. Zhu, T. Huang, Q. Zhang, M. Lein, and P. Lu, Reciprocal-space-trajectory perspective on high-harmonic generation in solids, Phys. Rev. Lett. **122**, 193901 (2019).

[22] L. Li, P. Lan, X. Zhu, and P. Lu, Huygens-fresnel picture for high harmonic generation in solids, Phys. Rev. Lett. **127**, 223201 (2021).

[23] T. Huang, L. Li, J. Li, X. Zhu, P. Lan, and P. Lu, Polarization-resolved analysis to solid high-order harmonic generation, J. Phys. B: At. Mol. Opt. Phys. **55**, 095601 (2022).

[24] L. Yue and M. B. Gaarde, Expanded view of electron-hole recollisions in solid-state high-order harmonic generation: Full-Brillouin-zone tunneling and imperfect recollisions, Phys. Rev. A **103**, 063105 (2021).

[25] T. Ikemachi, Y. Shinohara, T. Sato, J. Yumoto, M. Kuwata-Gonokami, and K. L. Ishikawa, Trajectory analysis of high-order-harmonic generation from periodic crystals, Phys. Rev. A **95**, 043416 (2017).

[26] P. G. Hawkins, M. Yu. Ivanov, and V. S. Yakovlev, Effect of multiple conduction bands on high-harmonic emission from dielectrics, Phys. Rev. A **91**, 013405 (2015).

[27] P. Xia, T. Tamaya, C. Kim, F. Lu, T. Kanai, N. Ishii, J. Itatani, H. Akiyama, and T. Kato, High-harmonic generation in GaAs beyond the perturbative regime, Phys. Rev. B **104**, L121202 (2021).

[28] P. Xia, C. Kim, F. Lu, T. Kanai, H. Akiyama, J. Itatani, and N. Ishii, Nonlinear propagation effects in high harmonic generation in reflection and transmission from gallium arsenide, Opt. Express **26**, 29393 (2018).

[29] M. Kolesik and J. V. Moloney, Numerical discreteness and dephasing in high-harmonic calculations in solids, Phys. Rev. B **108**, 115433 (2023).

[30] M. Kolesik, Assessment of tight-binding models for high-harmonic generation in zinc blende materials, Opt. Lett. **48**, 3191 (2023).

[31] J. Gu and M. Kolesik, Full-Brillouin-zone calculation of high-order harmonic generation from solid-state media, Phys. Rev. A **106**, 063516 (2022).

[32] Z. Long, H. Yang, K. Tian, L. He, R. Qin, Z.-Y. Chen, Q. J. Wang, and H. Liang, High-harmonic generation in CdTe with ultra-low pump intensity and high photon flux, Commun. Phys. **6**, 228 (2023).

[33] P. Vogl, H. P. Hjalmarson, and J. D. Dow, A semi-empirical tight-binding theory of the electronic structure of semiconductors, J. Phys. Chem. Solids **44**, 365 (1983).

[34] A. Di Carlo, Microscopic theory of nanostructured semiconductor devices: Beyond the envelope-function approximation, Semicond. Sci. Technol. **18**, R1 (2003).

[35] M. Fornari, H. H. Chen, L. Fu, R. D. Graft, D. J. Lohrmann, S. Moroni, G. P. Parravicini, L. Resca, and M. A. Stroscio, Electronic structure and wave functions of interface states in HgTe-CdTe quantum wells and superlattices, Phys. Rev. B **55**, 16339 (1997).

[36] J. Wilhelm, P. Grössing, A. Seith, J. Crewse, M. Nitsch, L. Weigl, C. Schmid, and F. Evers, Semiconductor Bloch-equations formalism: Derivation and application to high-harmonic generation from Dirac fermions, Phys. Rev. B **103**, 125419 (2021).

[37] R. E. F. Silva, F. Martín, and M. Ivanov, High harmonic generation in crystals using maximally localized Wannier functions, Phys. Rev. B **100**, 195201 (2019).